Accepted Manuscript

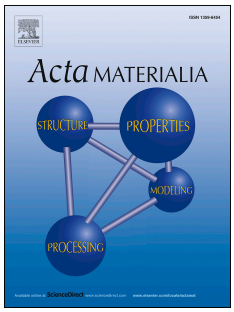

Charge carrier transport across grain boundaries in graphene

J.P. Mendez, F. Arca, J. Ramos, M. Ortiz, M.P. Ariza

PII: S1359-6454(18)30379-3

DOI: 10.1016/j.actamat.2018.05.019

Reference: AM 14572

To appear in: *Acta Materialia*

Received Date: 1 February 2018

Revised Date: 8 May 2018

Accepted Date: 10 May 2018

Please cite this article as: J.P. Mendez, F. Arca, J. Ramos, M. Ortiz, M.P. Ariza, Charge carrier transport across grain boundaries in graphene, *Acta Materialia* (2018), doi: 10.1016/j.actamat.2018.05.019.

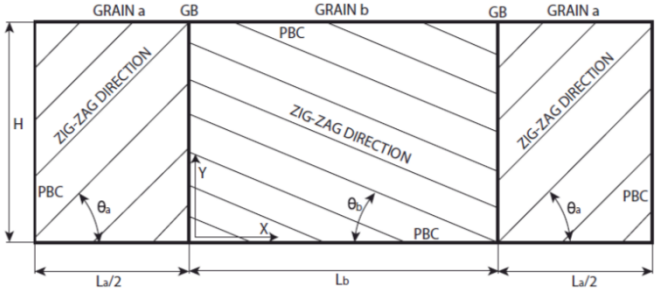

Geometry of the supercell

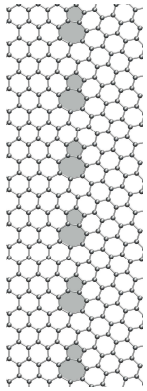

model I

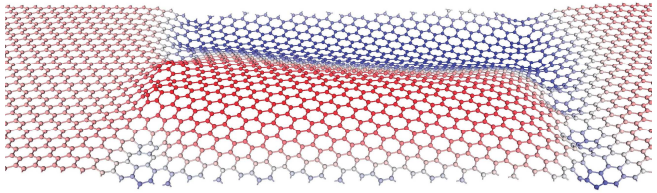

model II

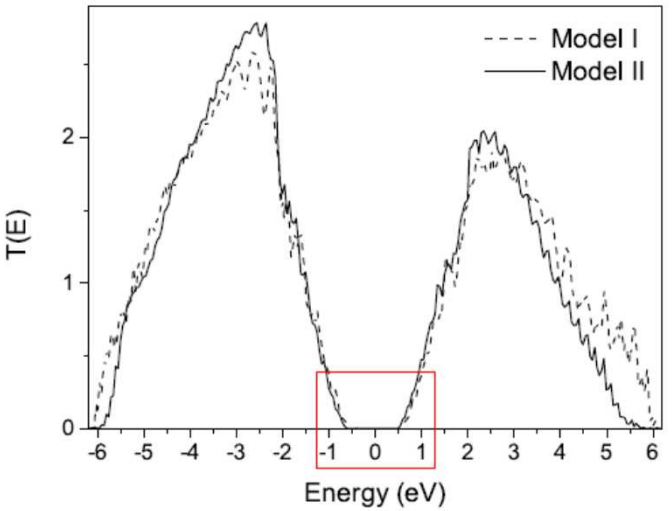

Charge carrier transport across grain boundaries in graphene

J. P. Mendez[a], F. Arca[b], J. Ramos[b], M. Ortiz[a], M. P. Ariza[b,*]

[a] *Division of Engineering and Applied Science, California Institute of Technology, CA 91125 Pasadena, USA*
[b] *Escuela Técnica Superior de Ingeniería, Universidad de Sevilla, Camino de los descubrimientos, s.n., 41092 Sevilla, Spain*

Abstract

We evaluate the charge carrier transmission across asymmetric grain boundaries (GB) in a graphene lattice within the Landauer-Büttiker formalism. We employ a tight-binding model for C-based materials that accounts for lattice strain introduced by topological defects, such as grain boundaries. In particular, we investigate electronic transmission across grain boundaries found to be stable up to high temperatures. Our calculations suggest that the introduction of GBs generally preserves the zero-transport gap property of pristine graphene. However, only some specific asymmetric GBs open a moderate transport gap, which can be as high as $\approx 1.15\ eV$. We find that the GBs that introduce a transport gap are characterized by the existence of a mismatch along the GB. Indeed, the magnitude of this mismatch appears to be the main structural variable that determines the transport gap size, with greater mismatch resulting in larger transport gaps. Finally, we find that the presence of GBs reduces considerably electron transmission, and less so hole transmission.

Keywords: Graphene, Charge carrier transport, Grain boundaries, Dislocations, Landauer-Büttiker formalism

1. Introduction

Owing to its high thermal mobility, above 4000 W/mK [1], its high electronic conductivity, above 15000 cm^2/Vs [2], its low mass density, $0.77 mg/m^2$, and its high breaking strength [3], graphene has elicited interest as a possible replacement for silicon in next-generation flexible electronic devices [4, 5]. However, pristine graphene has a zero band gap [6], which eliminates it right off as a candidate semiconductor material. For instance, thermoelectronic applications typically require semiconductor materials with band gaps in the range of 0.1eV and 0.4eV, whereas in photovoltaic applications the required band gap ranges from 1eV to 1.5eV [7]. Another important property of semiconductor materials is tunability, which enables them to cover a wider range of band gaps and greatly increases their range of application.

*Corresponding author
Email address: mpariza@us.es (M. P. Ariza)

A number of approaches have been proposed for opening the desired band gaps in graphene, e. g., strain [8, 9, 10], armchair nanoribbon configurations [11], doping [12, 13, 14] and engineered topological defects such as Stone-Wales defects, dislocations or grain boundaries [15, 16, 17]. Experimental and theoretical work [16, 18, 19, 7] has shown that the presence of randomly-distributed point defects modifies the electronic band structure only locally and results in a negligible band gap. By contrast, grain boundaries have been shown to introduce substantial transport gaps [15, 17].

Based on the momentum conservation principle, a theory of charge carrier transmission through GBs in graphene has been introduced by [15]. As a main result, they have distinguished two types of GBs, depending on the translation vector between the lattices on both sides of the grain boundary. These two types of GBs exhibit opposed behaviors, high transparency or perfect reflection with respect to charge carriers across GBs in a range of energies that can be quantified through a formula and is expressed in terms of the GB periodic vector. Furthermore, this theory was validated by the same authors using the Density Functional Theory (DFT) and the non-equilibrium Green's function (NEGF) formalism. Similarly, [17] found that the transport gap not only depends on the translation vector's relationship and the periodic length along the grain boundary, but also on the topology of the grain boundary.

In this work, in order to study the charge carrier transmission across GBs, we set forth a different approach which is based on the application of the Landauer-Büttiker (LB) formalism [20, 21, 22] in combination with a tight-binding (TB) model [23], allowing to account for the lattice strain introduced by the presence of grain boundaries within the graphene crystal. The LB formalism is based on coherent transport, i. e., only elastic scattering events are considered, whereas inelastic scattering events are assumed negligible. Previously, this computational framework has been widely used to investigate the electronic transport on different C-based materials, such as nanotubes, nanoribbons, among others. For instance, [24] studied the conductance of zig-zag and armchair nanoribbons including the presence of single defects and weak disorder at their edges; [25] investigated the effects of nanoconstrictions on the coherent transport in nanoribbons with zig-zag edges.

In contrast to the computational strategy adopted in this paper, the NEGF formalism [20] provides a general framework for the description of quantum transport with or without inelastic scattering events. However, it involves a substantial increase on the computational cost and complexity of the formulation, resulting in a consequent loss of computational efficiency. In the absence of inelastic interactions, both formalisms are equivalent. In this paper, we will show that the LB-TB model provides a fair compromise between accuracy and computational cost, and therefore, can be applied to situations which involve large number of atoms.

This work is organized as follows: in Section 2, we present different stable asymmetric grain boundaries; in Section 3, we introduce the Landauer-Büttiker formalism based on a tight-binding model; and in Section 4, based on this formalism, we will investigate the charge carrier transmission across GBs in graphene monolayers. General conclusions are summarized in Section 5 by way of closing.

2. Grain boundary structures in graphene

Engineered grain boundaries in 2D materials such as graphene provide an avenue for the design of materials with desirable properties, including transport gaps in applications to microelectronics. During the manufacturing process of graphene monolayers, meandering configurations of grain boundaries are formed spontaneously. In contrast to these unstructured and uncontrolled grain boundaries, here we focus on special grain boundaries that exhibit a regular and periodic structure in the form of regular arrays of point defects. In previous work, the authors have assessed the thermal stability of various grain boundary structures in graphene [26, 27], including symmetric and asymmetric configurations. Here we focus specifically on asymmetric grain boundaries since they have the strongest influence on electronic properties.

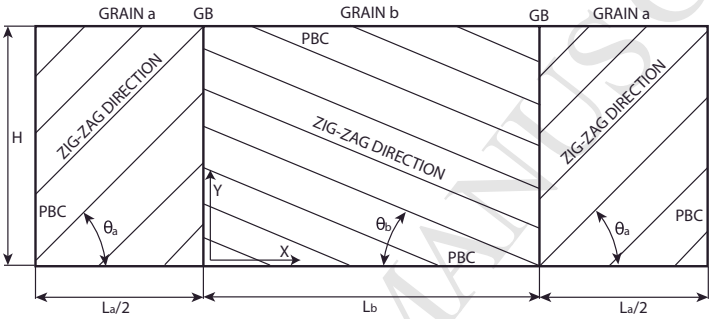

Figure 1: Geometry of the supercelll used to determine stable grain boundary configurations in polycrystalline graphene monolayers.

The orientations of two graphene grains, designated a and b, abutting on a grain boundary are determined by two in-plane angles θ_a and θ_b, Fig. 1. We adopt the convention that θ vanishes when the zig-zag direction of the graphene lattice coincides with the x-axis, Fig. 1. When $\theta_a = \theta_b$ the GB is symmetric, otherwise asymmetric. Symmetric GBs are fully characterized by their misorientation angle $\theta = \theta_a + \theta_b$. By contrast, asymmetric GBs have two independent degrees of freedom, θ_a and θ_b. Additionally, since we restrict attention to GBs consisting of a periodic array of dislocations [28], the GBs can also be described by the lattice coordinates $(n_a, m_a) \mid (n_b, m_b)$, of the periodic translation vectors $\mathbf{d}_a$ and $\mathbf{d}_b$ of the grains in the direction of the GB, cf. [28]. The translation vectors of the grains, $\mathbf{d}_a$ and $\mathbf{d}_b$, coincide for symmetric boundaries, but differ in asymmetric configurations. The requirement of periodicity restricts the possible misorientation angles between grains a and b, so that the difference between $\mathbf{d}_a$ and $\mathbf{d}_b$ remains small. Thus, H indicates the height of the computational cell, which is chosen to render the simulation computationally tractable while keeping the outlined boundary and geometric conditions. The length of the grains projected on the x-direction, L_a and L_b, respectively, are chosen so as to ensure periodicity.

We begin by characterizing the stability of periodic GB configurations and analyzing their geometries and formation energies. To this end, we perform calculations using SNL's Large-scale Atomic/Molecular Massively Parallel Simulator (LAMMPS), together with the AIREBO potential [29]. In the calculations,

Table 1: Geometric properties and formation energies of grain boundaries in polycrystalline graphene monolayers.

Angle θ	θ_a	θ_b	GB configuration (n_a,m_a) | (n_b,m_b)	H (Å)	Energy (eV/Å)	Energy [28] (eV/Å)
16.1°	16.1°	0°	(2,2)|(1,3)	8.5	0.427	0.482
17.2°	0°	17.2°	(13,4)|(9,9)	37.6	0.499	
36.6°	30°	6.6°	(4,0)|(3,2)	9.9	0.548	0.591
38.2°	8.2°	30°	(3,5)|(0,7)	16.9	0.483	0.457
30°	0°	30°	(0,5)|(3,3)-1	12.2	0.531	0.503
30°	0°	30°	(0,5)|(3,3)-2	62.8	0.505	
34.7°	30°	4.7°	(6,0)|(4,3)-1	14.6	0.451	
34.7°	30°	4.7°	(6,0)|(4,3)-2	14.6	0.535	0.575
34.7°	30°	4.7°	(6,0)|(4,3)-3	14.6	0.476	0.472

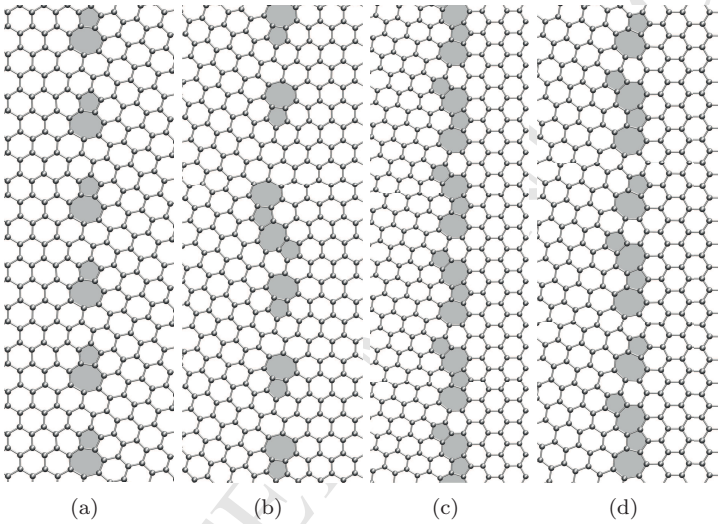

Figure 2: Observed structures of graphene GBs: (a) configuration (2,2)|(1,3) with θ=16.1°, (b) configuration (13,4)|(9,9) with θ=17.2°, (c) configuration (4,0)|(3,2) with θ=36.6°, and (d) configuration (5,0)|(3,3) with θ=38.2°.

we bring two grains in contact and allow the resulting GB to relax in the NVT ensemble at a temperature $\sim$ 0K, followed by relaxation in the NPT ensemble under zero in-plane presssure. Thus, the number of atoms in the supercells ranges from 380 atoms for GB (2,2)|(1,3), to 2,886 atoms for GB (0,5)|(3,3)-2.

Table 1 summarizes geometric properties and formation energies per unit length for the grain boundary configurations that are further investigated in Section 4. The list encompasses asymmetric GBs with misorientation angles ranging from 16.1° to 38.2°. All GBs under consideration have similar formation energies of the order of 0.5 eV/Å. Table 1 and Fig. 6 further compare our calculated formation energies with those obtained in earlier works [28, 30]. As may be seen, all calculated formation energies are in general overall good agreement, which provides a measure of verification.

The calculated equilibrium GB structures are shown in Figs. 2 and 3. We observe that configurations, (0,5)|(3,3) and (6,0)|(4,3), with misorientation angles 30° and 34.7°, respectively, present several isomers consisting of different

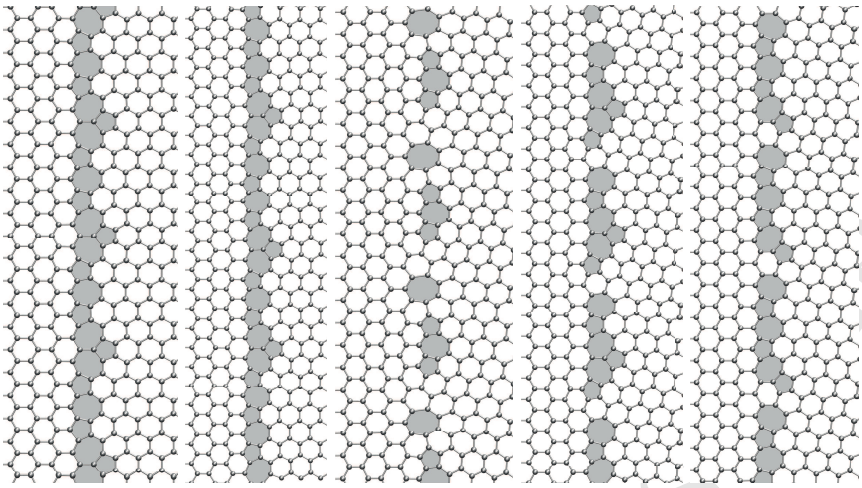

Figure 3: Observed atomic structures of graphene GBs: (a) configuration (0,5)|(3,3)-1 with θ=30°, (b) configuration (0,5)|(3,3)-2 with θ=30°, (c) configuration (6,0)|(4,3)-1 with θ=34.7° (d) configuration (6,0)|(4,3)-2 with θ=34.7°, and (e) configuration (6,0)|(4,3)-3 with θ=34.7°.

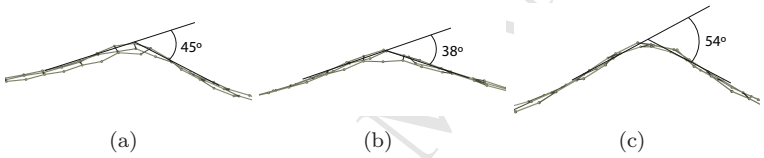

Figure 4: Inflection angles for some GB configurations: (a) (13,4)|(9,9), (b) (5,0)|(3,3) and (c) (6,0)|(4,3)-1.

arrangements of pentagons and heptagons, Fig. 3. In addition, the two isomers of GB (0,5)|(3,3) have substantially different repeat lengths, in contrast to the three isomers of GB (0,5)|(3,3), which have similar repeat lengths.

Remarkably, whereas these GB structures remain stable at finite temperature, out-of-plane warping localized at the 5-7 rings is observed starting at very low temperatures (see Fig. 4). The amplitude of the warping is in keeping with previous studies [28]. Moreover, when supercells of sufficient GB length are fully relaxed, the graphene layer develops a secondary wrinkled structure of larger periodicity than that the GB dislocations (Fig. 5). We return to the consequences of these wrinkled structure on transport properties in Section 4.

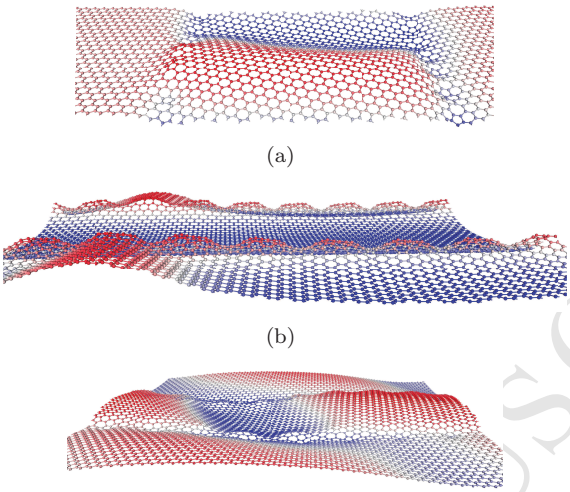

(a)

(b)

(c)

Figure 5: Equilibrium configuration of a parallel array of grain boundaries in graphene exhibiting a periodic distribution of 5-7 defects along the grain boundary together with a secondary wrinkle structure. (a) Configuration (2,2)|(1,3) with θ=16.1°, (b) configuration (6,0)|(4,3)-1 with θ=34.7° and (c) configuration (6,0)|(4,3)-2 with θ=34.7°.

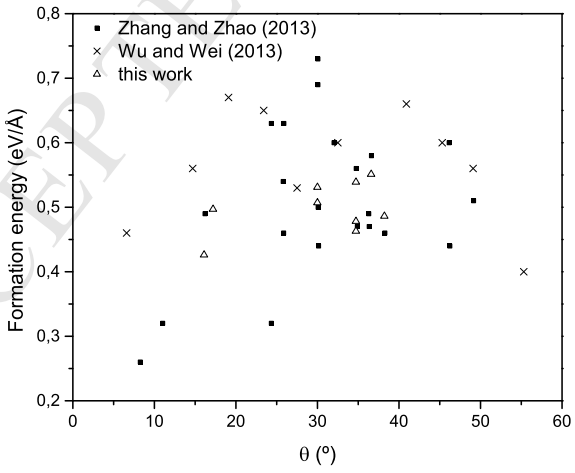

Figure 6: Grain boundary formation energy per unit length as a function of misorientation angle θ for various asymmetric GB configurations.

3. Model and methodology

The Landauer-Büttiker formalism supplies a simple framework for ascertaining the effect of GB structure on the electronic properties of polycrystalline graphene. We specifically investigate the properties of periodic arrays of parallel grain boundaries separating grains of various misorientations. We assume that the inelastic mean-free path of the electrons is much longer than any other characteristic dimensions of the model and, therefore, that the electron wave functions are coherent.

3.1. Model

The computational cell used in this work is shown in Fig. 7. The cell is composed of three regions: the left and right regions are perfect crystals of semi-infinite dimension in the x-direction and with periodic boundary conditions in the y-direction. The central region represents a periodic array of GBs separating crystals of two different orientations and has a finite width in the x-direction. The periodicity in the y-direction corresponds to an assumption of periodicity of the GB structure. As already noted, periodicity eliminates edge effects and renders the calculations computationally tractable. The distance L_b between two consecutive GBs is taken to be larger than 1.5 nm since GB interactions can be neglected at this distance [17]. The remaining distance L_a is chosen such that the lattice mismatch between the left (right) and central regions are negligible (see Fig. 1).

3.2. Landauer-Büttiker formalism

We briefly summarize the basis of the Landauer-Büttiker formalism for completeness and ease of reference (cf., e. g., [20, 21]). The tight-binding Hamiltonian matrix (TBHM) of the model sketched in Fig. 7 can be written in terms of submatrices as:

$$\boldsymbol{H} = \begin{pmatrix} \boldsymbol{H}_L & \boldsymbol{H}_{LC} & \boldsymbol{0} \\ \boldsymbol{H}_{CL} & \boldsymbol{H}_C & \boldsymbol{H}_{CR} \\ \boldsymbol{0} & \boldsymbol{H}_{RC} & \boldsymbol{H}_R \end{pmatrix}, \tag{1}$$

where $\boldsymbol{H}_C$ corresponds to the central component, $\boldsymbol{H}_{L(R)}$ corresponds to the isolated semi-infinite left (right) component and $\boldsymbol{H}_{L(R)C}$ represents the coupling between the left (right) and central regions of the model. Within the TB

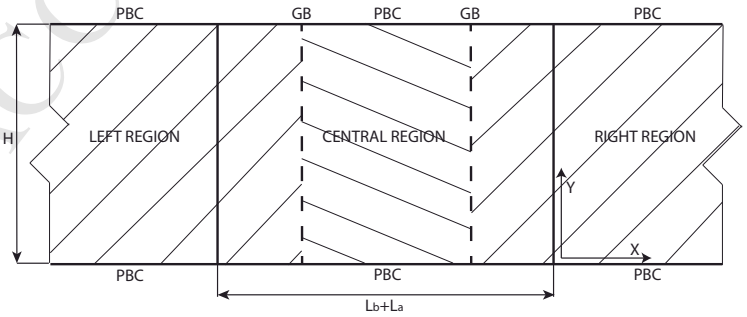

Figure 7: Geometry of the model used to compute the charge carrier transmission across GBs.

formalism, the empirical TBHM is obtained as

$$H_{l\alpha,j\beta} = E_\alpha \delta_{lj}\delta_{\alpha\beta} + h_{l\alpha,j\beta}(1 - \delta_{lj}\delta_{\alpha\beta}), \tag{2}$$

where l and j label atomic sites, α and β label atomic orbitals, and E_α and $h_{l\alpha,j\beta}$ are the on-site parameters and hopping functions, respectively.

For periodic systems such considered here Blochs theorem [31] applies. In $\boldsymbol{k}$-space, the sizes of the submatrices $\boldsymbol{H}_C(\boldsymbol{k})$, $\boldsymbol{H}_{L(R)}(\boldsymbol{k})$ and $\boldsymbol{H}_{L(R)C}(\boldsymbol{k})$ are $[N_c \times N_c]$, $[\infty \times \infty]$ and $[\infty \times N_c]$, respectively, where N_c is the number of atoms in the central region.

Following [20] and [21], the transmission function T across the central region at some energy E can be written as

$$T(E) = \frac{1}{N}\sum_{\boldsymbol{k}}^{N} Tr[\boldsymbol{\Gamma}_L(E,\boldsymbol{k})\boldsymbol{G}_C^\dagger(E,\boldsymbol{k})\boldsymbol{\Gamma}_R(E,\boldsymbol{k})\boldsymbol{G}_C(E,\boldsymbol{k})], \tag{3}$$

where $\boldsymbol{\Gamma}_L(E,\boldsymbol{k})$ and $\boldsymbol{\Gamma}_R(E,\boldsymbol{k})$ are the coupling $[N_c \times N_c]$ matrices, i. e., the coupling between the central and the left (right) regions, and $\boldsymbol{G}_C$ is the Green matrix of the central region. We recall that the transmission function gives the rate at which electrons are transmitted across the central region and, therefore, across the grain boundaries. For economy of notation, henceforth we drop the $\boldsymbol{k}$-dependence of the submatrices. The Green matrix of the central region, $\boldsymbol{G}_C$, follows readily as

$$\boldsymbol{G}_C(E) = [E^+\mathbb{I} - \boldsymbol{H}_C - \boldsymbol{\Sigma}_L(E) - \boldsymbol{\Sigma}_R(E)]^{-1} \approx [E\mathbb{I} - \boldsymbol{H}_C - \boldsymbol{\Sigma}_L(E) - \boldsymbol{\Sigma}_R(E)]^{-1}, \tag{4}$$

where $E^+ = E + i\eta$, with $\eta \to 0^+$, $\boldsymbol{\Sigma}_L$ and $\boldsymbol{\Sigma}_R$, are the self-energy $[N_c \times N_c]$ matrices corresponding to the left and right regions, respectively, and describe the effects of these regions on the electronic structure of the central region. We have

$$\boldsymbol{\Sigma}_l(E) = \boldsymbol{H}_{Cl}\boldsymbol{G}_l(E)\boldsymbol{H}_{lC}, \quad l = L, R, \tag{5}$$

where

$$\boldsymbol{G}_l(E) = (E^+\mathbb{I} - \boldsymbol{H}_l)^{-1}, \quad l = L, R. \tag{6}$$

are the Green functions of the semi-infinite left and right regions, respectively. It can be shown that the self-energy matrices, $\boldsymbol{\Sigma}_L(E)$ and $\boldsymbol{\Sigma}_R(E)$, can be further reduced to

$$\boldsymbol{\Sigma}_l(E) = \boldsymbol{H}_{Cl}\boldsymbol{G}_l^0(E)\boldsymbol{H}_{lC}, \quad l = L, R, \tag{7}$$

where $\boldsymbol{G}_L^0(E)$ and $\boldsymbol{G}_R^0(E)$ are the surface Green matrices of the left and right regions, respectively. In order to compute these matrices, we follow the recursive method of [24], [32] and [33]. Finally, the coupling matrices follow as

$$\boldsymbol{\Gamma}_l(E) = i(\boldsymbol{\Sigma}_l(E) - \boldsymbol{\Sigma}_l^\dagger(E)), \quad l = L, R. \tag{8}$$

i. e., are the difference between the retarded and the advanced self-energy matrices.

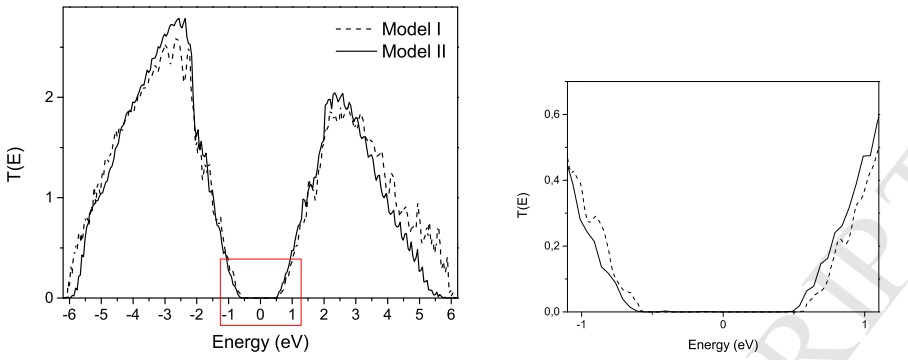

Figure 8: (a) Comparison of charge carrier transmission coefficient per shortest period across GBs when investigating flat (model I) or fully relaxed (model II) supercells of a GB with a misorientation angle of 16.1°, (b) detail of the transmission coefficient around zero energy. The Fermi level is set as zero.

4. Transmission across GBs in graphene

Using the computational framework just outlined, we proceed to investigate the transmission of charge carrier, electrons and holes, across periodic GB configurations under equilibrium conditions. In calculations we make two main approximations. Firstly, since three out of four valence electrons are located in the hybrid orbitals on the C atoms and interact with their counterparts on neighboring C atoms to form three σ-bonds that keep the electrons strongly localized within the lattice plane, only the p_z orbital is accounted for. Secondly, the fourth valence electron is located in the p_z orbital. This orbital is normal to the lattice plane and forms weak π-bonds with neighboring C atoms, which keeps the electron weakly bounded to the nuclei. Consequently, we assume that the p_z-electrons alone account for the electronic transport properties to a good approximation.

In calculations we employ the orthogonal TB model of [23] for C-based materials. This potential accounts for lattice strains [34, 35] by scaling the TB hopping integrals as in [36]. The TB model of [23] has been used extensively to compute the electronic properties of different C-based systems [37, 38, 39, 40]. We carry out the requisite numerical integrations over the Brillouin zone, Eq. (3), as a weighted sum over a grid of 576 k-points, with $\eta = 0.01$ for the parameter in Eq. (4). In order to assess convergence, we have carried out calculations using finer grids and smaller values of η. From this calculations, we verify that the numerical integration scheme used in calculations is accurate to 0.2%.

As already noted, the magnitude of the out-of-plane displacements in the neighborhood of GBs is small, of the order of the interatomic distance. Therefore, as a further simplification we restrict attention to flat simulation supercells. A comparison between flat supercell and fully-relaxed calculations, corresponding to a GB with a misorientation angle of 16.1°, is shown in Fig. 8. The figure compares the transmission curves obtained in both cases. As may be seen from the figure, the moderate out-of-plane warping of the lattice in the fully-relaxed does not significantly modify the charge carrier transmission curves, which have

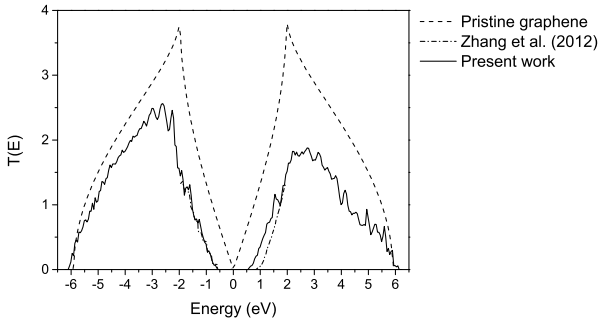

Figure 9: Transmission coefficient per period across GBs of the configuration with a misorientation angle of 16.1°. The Fermi level is set as zero.

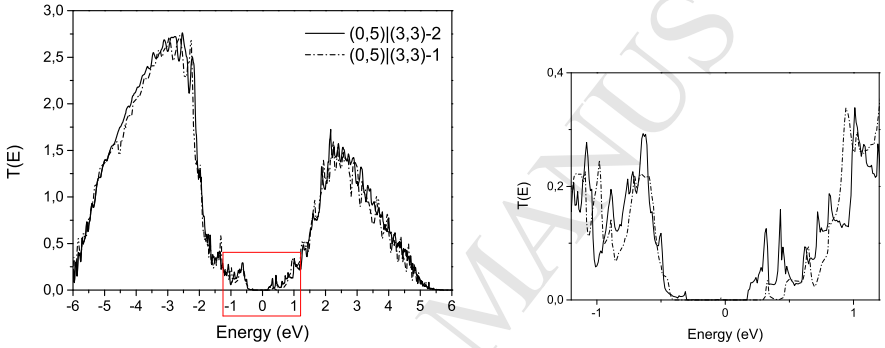

(a) (b)

Figure 10: (a) Comparison of charge carrier transmission coefficient per unit length (nm) across GBs of (0,5)|(3,3)-i configurations, (b) detail of the transmission coefficient around zero energy. The Fermi level is set as zero.

similar structure and display a nearly identical transport gap of 1.15 eV.

Fig. 9 compares the transmission values of the (2,2)|(1,3) GB obtained using DFT and nonequilibrium Green's function method [17] and the present approach by way of verification. Also shown for comparison are the transmission values pristine graphene. In agreement with [17, 15], the GBs are found to decrease the transmission coefficient over its entire range.

Our calculations are also in agreement with the analysis [17], concerned with the transport properties of three isomers of the (3,1)|(2,2) GB having almost identical period length. In this case, the transport gap is found to be influenced to some extent by the GB atomic structure and thus, does not depend exclusively on the periodic length along the grain boundary as proposed by [15]. As already described in Section 2, our calculations also reveal the existence of GB isomers. We find two isomers of the (0,5)|(3,3) GB of markedly different periodic length, 12.234 and 62.807 Å, respectively, and three isomers of the (6,0)|(4,3) GB of nearly the same period, 14.635, 14.603 and 14.605 Å, respectively. The computed transmission curves for the two isomers of the (0,5)|(3,3) GB and the three isomers of the (6,0)|(4,3) GB are shown in Figs. 10

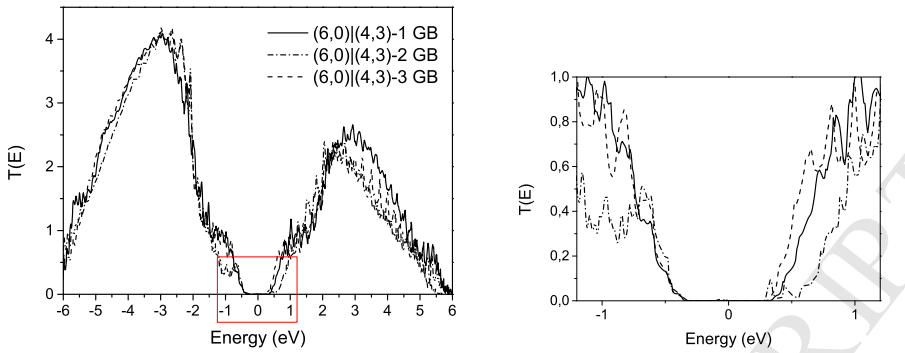

Figure 11: (a) Comparison of charge carrier transmission coefficient per period across GBs of (6,0)|(4,3)-i configurations, (b) detail of the transmission coefficient around zero energy. The Fermi level is set as zero.

Table 2: Transport gap (eV) of grain boundaries in polycrystalline graphene monolayers.

GB configuration	Transport gap (eV)	H (Å)	$\lvert\Delta d\rvert/d_{min}$ (%)
(2,2)|(1,3)	1.15	8.5	4.08
(13,4)|(9,9)	0.29	37.6	1.26
(4,0)|(3,2)	0.24	9.9	8.96
(3,5)|(0,7)	0.0	16.9	0.0
(0,5)|(3,3)-1	0.88	12.2	3.92
(0,5)|(3,3)-2	0.59	62.8	0.07
(6,0)|(4,3)-1	0.72	14.6	1.40
(6,0)|(4,3)-2	0.77	14.6	1.40
(6,0)|(4,3)-3	0.68	14.6	1.40

and 11, respectively. A comparison of these curves clearly indicates that the transport gap depends primarily on the periodic length and is relatively sensitive to the GB structure.

In Table 2 we summarize the values of the computed transport gaps for all GBs under consideration, together with their periodic length and lattice mismatch. As may be seen from these results, a wide range of transport gaps can be built in in graphene by means of GBs, up to ~ 1.15 eV for the $(1,3) \mid (2,2)$ GB ($\theta = 16.1°$). The emergence of transport gaps indicates that low-energy charge carriers can be blocked within a range of energy when transmitting across GBs. Furthermore, we observe that asymmetric GB configurations result in substantial transport gaps. They also result in localized strains along the grain boundaries due to a small lattice mismatch between the grains, i. e., $d_A \neq d_B$, cf. Section 2. This observation is in accordance with experimental and computational studies by [8] and [9], which suggest that band gaps in graphene appear as a consequence of asymmetric deformations. Consistently with this picture, the magnitude of the computed band gaps correlates closely with the lattice mismatch $|\Delta d|/d_{\min}$. In particular, as the mismatch increases the transport gap increases concomitantly. By contrast, the magnitude of the computed band gaps is relatively uncorrelated from the GB formation energy or the magnitude of its translation vector. These conclusions are also in agreement

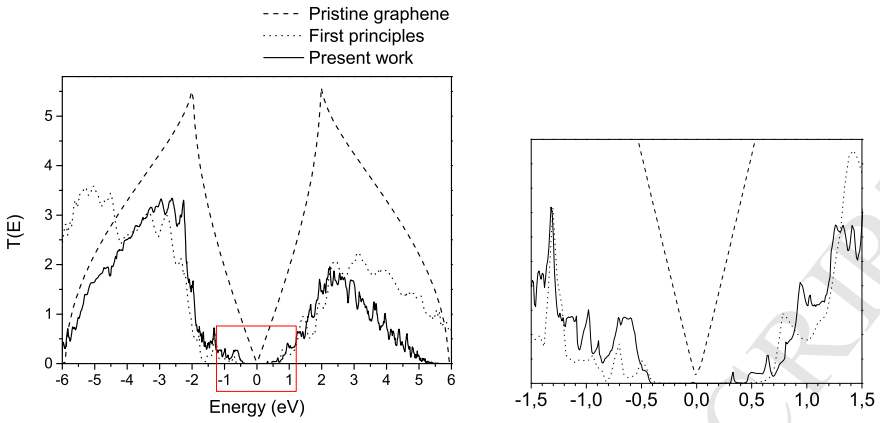

Figure 12: (a) Transmission coefficient per period across GBs of configuration (3,3)|(5,0)-1, (b) detail of the transmission coefficient around zero energy. The Fermi level is set as zero.

Table 3: Comparison of transport gap values of two GB configurations predicted by different authors.

Misorientation angle $\theta(^\circ)$	30°	16.1°
GB configuration	(0,5)|(3,3)	(1,3)|(2,2)
This work	0.88	1.15
Reference [17]	1.03	1.45
Reference [15]	1.04	-
Theoretical gap (E_g(eV)$\approx \frac{1.38}{d(\mathrm{nm})}$) [15]	1.11	1.59

with the analysis of [17]. Finally, we observe that the electron-hole symmetry of the transmission curve is broken by the presence of grain boundaries. In addition, the transmission of holes is considerably higher across the grain boundaries than the transmission of electrons. This symmetry breaking has also been observed in graphene containing topological defects such as Stone-Wales defects or dislocations [19].

Finally, for purposes of validation we have carried out DFT and NEGF calculations using the SIESTA and TRANSIESTA codes [41, 42]. The calculations employ the generalized gradient approximation [43], along with the double-ξ plus polarization basis set, the non-conserving pseudopotential [44] and a mesh cutoff of 400 R_y. The results of these calculations are included as dot lines in Figs. 12 and 13 by way of comparison. The good agreement between the first-principles and TB calculations is evident from this comparison. In general, our results are also in good agreement with previous studies based on DFT and the NEGF formalism [15, 17], although our calculations predict somewhat lower transport gaps for the GB configurations reported in Table 3.

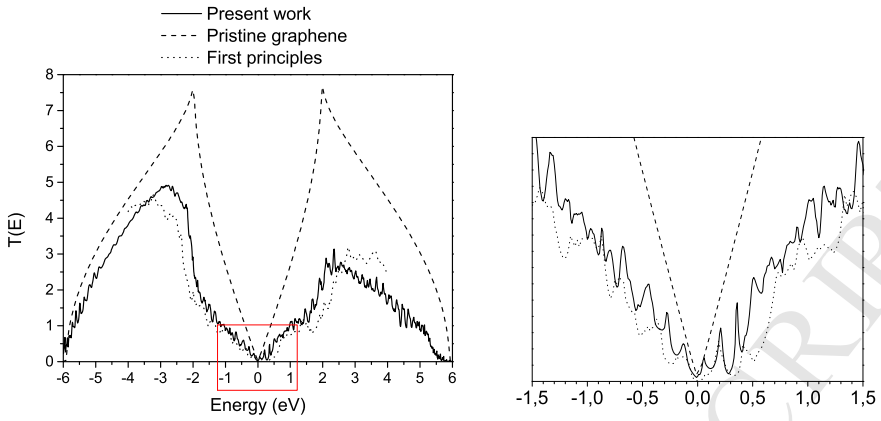

Figure 13: (a) Transmission coefficient per period across GBs of configuration (7,0)|(5,3), (b) detail of the transmission coefficient around zero energy.

5. Conclusions

We have evaluated the charge carrier transmission across asymmetric grain boundaries (GB) in graphene lattice within the Landauer-Büttiker formalism [20, 21]. We employ a tight-binding model for C-based materials [23] that accounts for lattice strain introduced by topological defects, such as grain boundaries. In particular, we have investigated the electronic transmission across grain boundaries found to be stable up to high temperatures [26, 27]. Our calculations suggest that GBs generally preserve the semiconductor properties of pristine graphene, but only some specific asymmetric GBs open a moderate transport gap. For asymmetric configurations such as the $(1,3)$ | $(2,2)$ GB ($\theta = 16.1°$), the resulting transport gap can be as high as ≈ 1.15 eV. We find that the GBs that introduce a transport gap are characterized by the existence of a mismatch along the GB. Indeed, the magnitude of this mismatch ($|\Delta d|/d_{\min}$) appears to be the main structural variable that determines the transport gap size, with greater mismatch resulting in larger transport gaps. Finally, we find that the presence of GBs reduces considerably electron transmission, and less so hole transmission.

Acknowledgments

We gratefully acknowledge the support of the Ministerio de Educación, Cultura y Deporte of Spain (FPU2009) and the Consejería de Economía, Innovación, Ciencia y Empleo of Junta de Andalucía (P12-TEP-850).

References

[1] A. A. Balandin, S. Ghosh, I. Bao, W.and Calizo, D. Teweldebrhan, F. Miao, C. Lau, Superior thermal conductivity of single-layer graphene, Nano Letters 8 (3) (2008) 902–907.

[2] A. K. Geim, K. S. Novoselov, The rise of graphene, Nature Materials 6 (3) (2007) 183–191.

[3] C. Lee, X. Wei, J. Kysar, J. Hone, Measurement of the elastic properties and intrinsic strength of monolayer graphene 321 (5887) (2008) 385–388.

[4] S. Bae, H. Kim, Y. Lee, X. Xu, J. Park, Y. Zheng, J. Balakrishnan, T. Lei, H. R. Kim, Y. I. Song, Y. Kim, K. Kim, B. zyilmaz, J. Ahn, B. H. Hong, S. Iijima, Roll-to-roll production of 30-inch graphene films for transparent electrodes, Nature Nanotechnology 5 (8) (2010) 574–578.

[5] Y. Jung, K. Park, S. Hur, S. Choi, S. Kang, High-transmittance liquid-crystal displays using graphene conducting layers, Liquid Crystals 0 (0) (2013) 1–5.

[6] K. S. Novoselov, A. K. Geim, S. V. Morozov, D. Jiang, Y. Zhang, S. V. Dubonos, I. V. Grigorieva, A. A. Firsov, Electric field effect in atomically thin carbon films 306 (5696) (2004) 666–669.

[7] A. Castellanos-Gomez, Black phosphorus: Narrow gap, wide applications, The Journal of Physical Chemistry Letters 6 (21) (2015) 4280–4291.

[8] Z. H. Ni, T. Yu, Y. H. Lu, Y. Y. Wang, Y. P. Feng, Z. X. Shen, Uniaxial strain on graphene: Raman spectroscopy study and band-gap opening, ACS Nano 2 (11) (2008) 2301–2305.

[9] G. Gui, J. Li, J. Zhong, Band structure engineering of graphene by strain: First-principles calculations, Phys. Rev. B 78 (2008) 075435.

[10] J. Zhang, K. P. Ong, P. Wu, The influence of out-of-plane deformation on the band gap of graphene nanoribbons, The Journal of Physical Chemistry C 114 (29) (2010) 12749–12753.

[11] N. Nemec, Quantum transport in carbon-based nanostructures, Ph.D. thesis (2007).

[12] P. A. Denis, Band gap opening of monolayer and bilayer graphene doped with aluminium, silicon, phosphorus, and sulfur, Chemical Physics Letters 492 (46) (2010) 251 – 257.

[13] A. Bhattacharya, S. Bhattacharya, G. Das, Strain-induced band-gap deformation of h/f passivated graphene and h-bn sheet, Physical Review B 84 (7) (2011) 075454.

[14] P. Rani, V. Jindal, Designing band gap of graphene by b and n dopant atoms, RSC Advances 3 (3) (2013) 802–812.

[15] O. Yazyev, S. Louie, Electronic transport in polycrystalline graphene, Nat Mater 9 (2010) 806–809.

[16] S. N. Shirodkar, U. V. Waghmare, Electronic and vibrational signatures of stone-wales defects in graphene: First-principles analysis, Phys. Rev. B 86 (2012) 165401.

[17] J. Zhang, J. Gao, L. Liu, J. Zhao, Electronic and transport gaps of graphene opened by grain boundaries, Journal of Applied Physics 112 (5) (2012) 053713.

[18] A. Lherbier, S. Dubois, X. Declerck, Y. Niquet, S. Roche, J. Charlier, Transport properties of graphene containing structural defects, Physical Review B 86 (2012) 075402.

[19] J. P. Mendez, M. P. Ariza, Harmonic model of graphene based on a tight binding interatomic potential, Journal of the Mechanics and Physics of Solids 93 (2016) 198–223.

[20] S. Datta, Electronic Transport in Mesoscopic Systems, Cambridge University Press, Cambridge, 1995.

[21] S. Datta, Quantum transport: Atom to Transistor, Cambridge University Press, Cambridge, 2005.

[22] L. Foa Torres, S. Roche, J. Charlier, Introduction to Graphene-Based Nanomaterials:From Electronic Structure to Quantum Transport, Cambridge University Press, Cambridge, 2014.

[23] C. H. Xu, C. Z. Wang, C. T. Chan, K. M. Ho, A transferable tight-binding potential for carbon, Journal of Physics: Condensed Matter 4 (28) 6047.

[24] T. C. Li, S.-P. Lu, Quantum conductance of graphene nanoribbons with edge defects, Phys. Rev. B 77 (2008) 085408.

[25] F. Munoz-Rojas, D. Jacob, J. Fernandez-Rossier, J. J. Palacios, Coherent transport in graphene nanoconstrictions, Phys. Rev. B 74 (2006) 195417.

[26] J. P. Mendez, F. Macias, M. P. Ariza, Thermal stability of tilt grain boundaries in graphene, in: Applied Mechanics and Materials, Vol. 481, Trans Tech Publ, 2014, pp. 129–132.

[27] J. P. Mendez, F. Arca, M. P. Ariza, Stability of asymmetric grain boundaries in graphene, in: ECCOMAS Congress 2016 - Proceedings of the 7th European Congress on Computational Methods in Applied Sciences and Engineering, Vol. 1, 2016, pp. 188–196.

[28] Z. Zhang, J. Zhao, Structures and electronic properties of symmetric and nonsymmetric graphene grain boundaries, Carbon 55 (2013) 151–159.

[29] S. J. Stuart, A. B. Tutein, J. A. Harrison, A reactive potential for hydrocarbons with intermolecular interactions, J. Chem. Phys. 112 (14) (2000) 6472–6486.

[30] J. Wu, Y. Wei, Grain misorientation and grain-boundary rotation dependent mechanical properties in polycrystalline graphene, Journal of the Mechanics and Physics of Solids 61 (2013) 14211432.

[31] C. Kittel, Introduction to Solid State Physics, 8th Edition, John Wiley & Sons, Inc., New York, 2004.

[32] D. L. John, D. L. Pulfrey, Green's function calculations for semi-infinite carbon nanotubes, physica status solidi (b) 243 (2).

[33] M. P. L. Sancho, J. M. L. Sancho, J. M. L. Sancho, J. Rubio, Highly convergent schemes for the calculation of bulk and surface green functions, Journal of Physics F: Metal Physics 15 (4) (1985) 851.

[34] E. Cadelano, P. L. Palla, S. Giordano, L. Colombo, Nonlinear elasticity of monolayer graphene, Phys. Rev. Lett. 102 (2009) 235502.

[35] E. Cadelano, S. Giordano, L. Colombo, Interplay between bending and stretching in carbon nanoribbons, Phys. Rev. B 81 (2010) 144105.

[36] L. Goodwin, A. J. Skinner, D. G. Pettifor, Generating transferable tight-binding parameters: Application to silicon, EPL (Europhysics Letters) 9 (7) 701.

[37] A. A. Farajian, M. Mikami, Electronic and mechanical properties of c 60 -doped nanotubes, Journal of Physics: Condensed Matter 13 (35) (2001) 8049.

[38] S. Souma, Y. Ohmi, M. Ogawa, Effect of lateral strain on gate induced control of electrical conduction in single layer graphene device, Journal of Computational Electronics 12 (2) (2013) 170–174.

[39] N. Gorjizadeh, Y. Kawazoe, A. A. Farajian, Electronic and Transport Properties of Defected Graphene Nanoribbons, Physics and Applications of Graphene - Theory, InTech, Croatia, 2011.

[40] A. D. Smith, S. Vaziri, F. Niklaus, A. C. Fischer, M. Sterner, A. Delin, M. stling, M. C. Lemme, Pressure sensors based on suspended graphene membranes, Solid-State Electronics 88 (2013) 89 – 94.

[41] J. M. Soler, E. Artacho, J. D. Gale, A. Garca, J. Junquera, P. Ordejn, D. Snchez-Portal, The siesta method for ab initio order-n materials simulation, Journal of Physics: Condensed Matter 14 (11) 2745.

[42] M. Brandbyge, J. L. Mozos, P. Ordejón, J. Taylor, K. Stokbro, Density-functional method for nonequilibrium electron transport, Phys. Rev. B 65 (2002) 165401.

[43] J. Perdew, K. Burke, M. Ernzerhof, Generalized gradient approximation made simple, Phys. Rev. Lett. 77 (1996) 3865–3868.

[44] N. Troullier, J. Martins, Efficient pseudopotentials for plane-wave calculations, Phys. Rev. B 43 (1991) 1993–2006.